Temperature and anisotropic-temperature relaxation measurements in cold, pure-electron plasmas

B. R. Beck
Lawrence Livermore National Laboratory L-421, Livermore, California 94550

J. Fajans
Department of Physics, University of California, Berkeley, Berkeley, California 94720

J. H. Malmberg[a)]
Department of Physics, University of California, San Diego, La Jolla, California 92093

(Received 30 October 1995; accepted 3 January 1996)

Plasma temperatures in the range 25 to 2×10^6 K have been measured using a cryogenic, ultra-high vacuum, pure-electron plasma trap. The rate ν at which the temperatures parallel and perpendicular to the applied magnetic field relax to a common value has been measured over the temperature range 28 to 3.8×10^5 K and the magnetic field range 20 to 60 kG. This rate ν is closely related to the plasma collision frequency. When the cyclotron radius r_c is large compared to the classical distance of closest approach b ($r_c/b\gg1$), the measured values of ν are in agreement with conventional collision theory. When the cyclotron radius is small compared to the classical distance of closest approach ($r_c/b\ll1$), ν drops precipitously as r_c/b is decreased, in agreement with the many-electron adiabatic invariant theory of O'Neil and Hjorth. © *1996 American Institute of Physics.* [S1070-664X(96)00604-0]

I. INTRODUCTION

Plasmas consisting of a single-charge species are the subject of much current research.[1,2] Since recombination cannot occur in these plasmas, they can be cooled to very low temperatures. Using a cryogenic, ultra-high vacuum apparatus we have obtained pure-electron plasmas with temperatures ranging from 25 to 2×10^6 K. In conjunction with an applied magnetic field varying from 20 to 60 kG, this temperature range puts our plasmas in the large and, in part, unique parameter regime, $1/35\lesssim r_c/b\lesssim10^6$. Here r_c is the cyclotron radius, $b=e^2/(\kappa T)$ is the classical distance of closest approach, e is the charge of an electron, κ is Boltzmann's constant, and T is the plasma temperature. The plasma temperatures parallel and perpendicular to the magnetic field need not be equal, and, when unequal, we have measured the relaxation rate ν at which electron–electron collisions equilibrate these temperatures. Such relaxation is one of the basic plasma collisional processes.[3] We find that in the high temperature, weakly magnetized regime $r_c/b\gg1$ the measured relaxation rate is proportional to $T^{-3/2}$. The measured rate peaks for temperatures where $r_c/b\sim1$. As the temperature is lowered further, the plasmas enter the strongly magnetized regime $r_c/b\ll1$, where the relaxation rate drops precipitously as the temperature is decreased. This drop is in agreement with the theoretical prediction of O'Neil and Hjorth.[4]

In Fig. 1 we show our relaxation rate data combined with data obtained by Hyatt, Driscoll and Malmberg.[5,6] In this figure we have plotted the normalized relaxation rate $\nu/(nb^2\bar{v})$ versus r_c/b, where n is the plasma density, $\bar{v}=\sqrt{\kappa T/m}$ is the average velocity and m is the electron mass. The solid curve is a Monte Carlo-based prediction due to Glinsky *et al.*;[7] no adjustable parameters are used in calculating this curve.

In Section II we describe our pure-electron plasma apparatus and how we create and trap pure-electron plasmas. In Section III we discuss the results of plasma cooling via cyclotron radiation. In Section IV we present our relaxation rate measurement procedure and data. In Appendix A we discuss our density measurement, and in Appendix B we discuss our temperature diagnostic. In Appendix C we discuss the procedure used by Hyatt, Driscoll and Malmberg[5,6] to measure the relaxation rate for the regime $3\times10^4\lesssim r_c/b\lesssim10^6$.

II. APPARATUS

The simplified schematic of our electron trap shown in Fig. 2 contains the basic elements needed for trap operation: the electron source, three collimated, cylindrical electrodes, and five charge collectors. All trap elements are aligned with a strong static magnetic field. The actual electron trap includes additional collimated, cylindrical electrodes. All the electrodes have a wall radius of $R_w=1.27$ cm. The trap is sealed into an evacuated vessel, and the entire assembly is cooled to liquid helium temperature (4.2 K). Cooling the trap accomplishes two objectives: first, the cold trap surfaces cryopump the background gas to densities measured to be less than 10^5 cm^{-3}. Second, in the absence of any heating mechanisms, cyclotron radiation will eventually cause the plasma to cool to 4.2 K.

The static magnetic field confines the plasma radially.[8] The well created by biasing the two end electrodes ($\mathbf{G}_1$ and $\mathbf{G}_3$) sufficiently negatively relative to the central electrode ($\mathbf{G}_2$) confines the electrons axially. For simplicity, we assume that the confining electrodes are $\mathbf{G}_1$ and $\mathbf{G}_3$ throughout this paper; more generally, any of the trap electrodes, including those not shown in Fig. 2, can be used

[a)]Deceased.

 1070-664X/96/3(4)/1250/9/$10.00

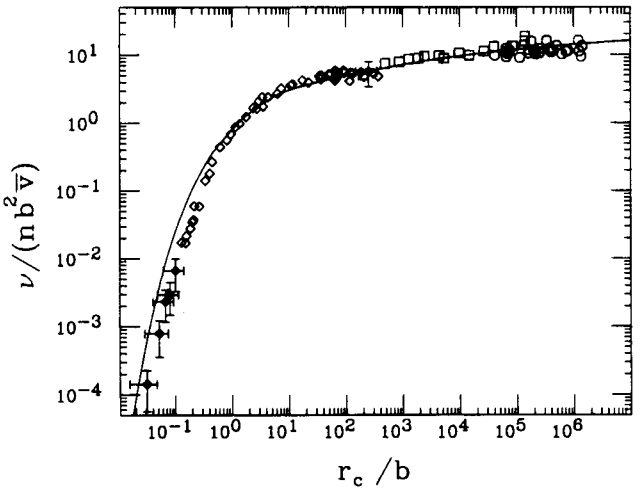

FIG. 1. Normalized relaxation rate $[\nu/(nb^2\bar{v})]$ vs. cyclotron radius divided by distance of closed approach (r_c/b). The diamond points ◇ were obtained using the balanced heating technique, square points □ were obtained using the unbalanced technique, and the circular points ○ are data obtained by Hyatt, Driscoll and Malmberg. The solid curve is the Glinsky *et al.* Monte Carlo prediction.

as a confinement electrode, thereby allowing the plasma length l to range from about 1 cm to about 10 cm. Here plasma length refers to an average axial dimension of the plasma.

The trap is operated with repeated cycles consisting of capture, manipulate, and release/dump phases. A cycle begins with the central electrode ($\mathbf{G}_2$) grounded and the two end electrodes ($\mathbf{G}_1$, $\mathbf{G}_3$) at -100 V. During the capture phase the left-most electrode ($\mathbf{G}_1$) is momentarily grounded, allowing electrons to flow from the negatively biased, hot-tungsten-filament electron source[9] to the center of the trap. This electrode ($\mathbf{G}_1$) is then biased negatively to trap the plasma in the center electrode ($\mathbf{G}_2$). Next, during the manipulate phase, the plasma is held for a variable length of time while various plasma manipulations are performed. Finally, during the dump phase, the plasma is allowed to flow out of the trap along the magnetic field lines by grounding $\mathbf{G}_3$. The dumped plasma is captured on the charge collection plates $\mathbf{C}_1$ through $\mathbf{C}_5$, and the resulting charge and current time-profile yield the plasma density and temperature information respectively. The time between capture and release is called the confinement time, t_c, and can range from 1 ms to more than 40,000 s, but is typically on the order of 10 s.

Since most measurements are obtained by releasing the plasma onto the charge collection plates, we usually obtain only one measurement per plasma. Many of our results rely on the analysis of thousands of cycles; consequently, good cycle-to-cycle reproducibility of the plasmas is critical. When the experimental parameters are properly adjusted, the cycle-to-cycle variation of the charge measured on each collector is at most 2% of the total charge. The cycle-to-cycle variation of the temperature for nominally identical plasmas is about 1% at high temperatures and somewhat higher at lower temperatures. However, this does not mean that the temperature measurement is accurate to 1% since systematic errors may be as large as 10% for high temperatures and larger for low temperatures.

The plasmas cannot be confined indefinitely. Anomalous loss mechanisms[10] cause the plasmas to expand radially (albeit slowly); thus the charge measured on the innermost charge collection plate $\mathbf{C}_1$ decreases as the containment time is increased. We define the lifetime of a plasma to be the containment time t_c at which the charge measured on $\mathbf{C}_1$ is one half the charge measured when $t_c = 1$ s. Depending on magnetic field, plasma length and plasma density, the measured lifetime ranges from about 100 s to greater than 10^5 s. In general, plasma lifetime increases when (1) the magnetic field is increased, (2) the plasma length is decreased, or (3) the plasma density is decreased. This relationship between magnetic field, plasma length and lifetime is in qualitative agreement with that found by Driscoll, Fine and Malmberg.[10]

Since our plasmas are unneutralized, they induce a radial electric field E_r, which, in conjunction with the axial magnetic field, cause the plasma electrons to **E×B** drift. The net effect is that the plasma rotates about the z-axis with frequency $\omega_E(r) = cE_r/(rB)$, where r is the radius from the axis, and c is the speed of light. Recent results[11] indicate that large θ variations in the density profile disappear on a time scale of several hundred ω_E^{-1}. For plasmas in this study $\omega_E^{-1} \sim 1$ μs. After trapping a plasma we always wait at least 100 ms before proceeding; this allows the plasma to come into local thermal equilibrium (i.e. it allows the plasma distribution to relax to a Boltzmann distribution along the z axis). Since 100 ms is about 10^5 ω_E^{-1} we believe that both the plasma density and the plasma temperature are, to a good approximation, azimuthally symmetric.

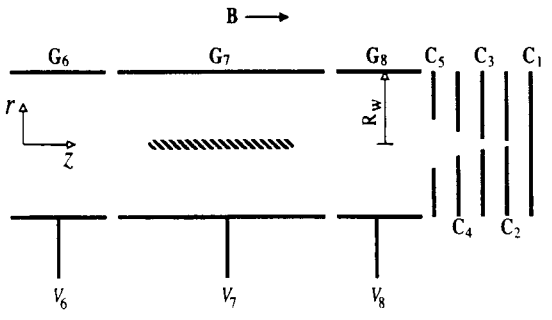

FIG. 2. Schematic of the confinement apparatus showing a confined plasma.

III. PLASMA TEMPERATURE MEASUREMENTS

Our plasmas are created with a temperature of approximately 10^4 K. We obtain hotter plasmas by pushing the plasma off a potential hill, and we obtain colder plasmas by employing cyclotron-radiation cooling. Note that the temperature associated with the degree of freedom parallel to the magnetic field, $T_\parallel$, and the temperature associated with the degree of freedom perpendicular to the magnetic field, $T_\perp$, need not be equal. In addition, each temperature may be a function of radius and time [e.g. $T_\parallel = T_\parallel(r,t)$]. However, since we always measure plasma temperatures after the plas-

mas have been quiescent for a time which is long compared to a collision time, we believe that $T_{\|}(r,t)$ will have equilibrated with $T_{\perp}(r,t)$ at the time our temperature measurements are made.

A. Cyclotron radiation cooling theory

A single classical electron, orbiting in a magnetic field, loses energy via cyclotron radiation at a rate given by the Larmor formula:

$$\frac{dE_{\perp}}{dt}=\frac{2e^2}{3c^3}a_{\perp}^2=\frac{4e^2\Omega^2}{3mc^3}E_{\perp}, \tag{1}$$

where $a_{\perp}=\Omega v_{\perp}$ is the perpendicular acceleration, Ω is the cyclotron frequency, and $E_{\perp}$ is the perpendicular energy $mv_{\perp}^2/2$. Averaging Eq. (1) over a Maxwellian distribution yields

$$\frac{dT_{\perp}}{dt}=-\frac{3T_{\perp}}{2\tau_r}, \tag{2}$$

where the radiation time τ_r is defined to be

$$\tau_r\equiv\frac{9mc^3}{8e^2\Omega^2}\simeq\frac{4\times10^8}{B^2}\ \text{s}. \tag{3}$$

When $\nu\gg\tau_r^{-1}$, as is the case for our plasmas, and the plasma is quiescent, then $T_{\perp}(t)=T_{\|}(t)=T(t)$ to a good approximation, and one obtains

$$\frac{dT}{dt}=\frac{-T}{\tau_r}. \tag{4}$$

The factor of 3/2 in the right hand side of Eq. (2) disappears from Eq. (4) because the two perpendicular degrees of freedom dissipate the energy contained in all three degrees of freedom.

Equation (4) is strictly applicable only when the temperature of the surrounding heat bath is much less than the plasma temperature, and when quantum effects are negligible. Inclusion of both of these effects slow the cooling, and modify Eq. (4) to[12]

$$\frac{dT}{dt}=-\frac{T}{\tau_r}R\left(\frac{\hbar\Omega}{\kappa T},\frac{\hbar\Omega}{\kappa T_w}\right), \tag{5}$$

where

$$R(x,y)=x\frac{\exp(y)-\exp(x)}{[\exp(y)-1][\exp(x)-1]}. \tag{6}$$

The heat bath correction is important only when the plasma has cooled to near the heat bath temperature, and the quantum correction is important only when a substantial fraction of the electrons are in their nonradiating lowest Landau level, i.e. when $\kappa T\approx\hbar\Omega$. Practically speaking, these corrections are relevant only at the very coldest temperatures that we can measure.

B. Cyclotron radiation cooling results

The measured and predicted [Eq. (5)] plasma temperatures vs. time are shown in Fig. 3. The temperature at $t=0$, necessary for the solution of T in Eq. (5), is obtained from

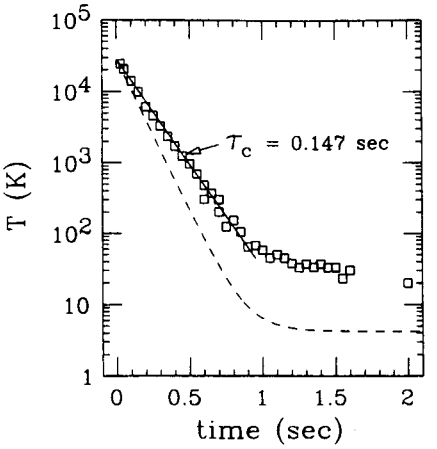

FIG. 3. Measured plasma temperature vs. time for a magnetic field of 61.3 kG. The dashed curve is a plot of Eq. (5).

the experimental data. Initially, the measured temperature decays exponentially with a time constant of $\tau_c=0.147$ s. Here $\tau_c\equiv T^{-1}dT/dt$ is computed in the high temperature regime. The calculation of the predicted cooling rate [Eq. (3)] ignores plasma opacity and waveguide effects.[13,14] Nonetheless, the measured cooling time is within 30% of the predicted rate. At about 50 K, the measured temperature deviates from exponential decay, but continues to cool to about 20 K. This decrease in the cooling rate could be due either to an unknown heating mechanism, or to increasing errors in the temperature measurement at low temperature. The decrease occurs at too high a temperature to be explained by quantum or heat bath effects. Figure 4 shows the measured and predicted [Eq. (3)] cooling times versus magnetic field.

IV. RELAXATION RATE MEASUREMENT

We determine the relaxation rate by measuring the change in the temperature, and hence the net work done on the plasma, after the plasma undergoes several compression/expansion cycles. Collisions make these cycles irreversible, and the net work done on the plasma is maximized when the frequency of the compression cycles is comparable to the relaxation frequency.

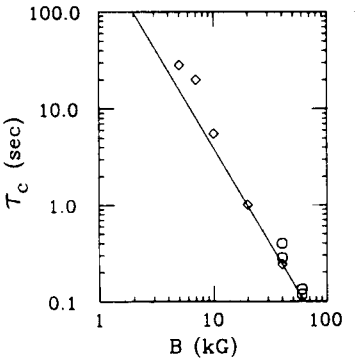

FIG. 4. Measured cyclotron radiative cooling time τ_c vs. magnetic field B. The solid curve is a plot of Eq. (3).

The plasma is compressed by sinusoidally modulating the potential on the confining electrode G_1, thereby doing work against the axial plasma pressure. This pressure is the sum of the kinetic and electrostatic potential pressures. For our plasmas, the potential pressure is much larger than the kinetic pressure. However, since our plasmas are weakly correlated ($e^2 n^{1/3}/(\kappa T) \ll 1$) and since the plasma compression is done quasistatically ($f \ll \bar{\omega}_p$ where $\bar{\omega}_p$ is the frequency of the lowest plasma mode), the potential pressure does not directly effect the kinetic pressure.[15,16] Consequently, the kinetic pressure is well described by the ideal gas law and the work done to the kinetic energy by the compression is given by $dW = -P_\parallel dV = -n\kappa T_\parallel A dl$. Here A is the cross-sectional area of the plasma that is perpendicular to the length change and dl is the average differential change in the plasma length. The rate of change of the average axial kinetic energy per particle due to the compression is

$$\frac{1}{N}\frac{dW}{dt} = -\frac{An}{N}\frac{dl}{dt}\kappa T_\parallel = \frac{1}{l}\frac{dl}{dt}\kappa T_\parallel . \tag{7}$$

Incorporating Eq. (7) and a cyclotron cooling term [Eq. (2)] into the standard definitions[17] for ν, one obtains the coupled equations

$$\frac{dT_\perp}{dt} = \nu(T_\parallel - T_\perp) - \frac{3T_\perp}{2\tau_r} \tag{8}$$

and

$$\frac{dT_\parallel}{dt} = 2\nu(T_\perp - T_\parallel) - 2\frac{T_\parallel}{l}\frac{dl}{dt}. \tag{9}$$

The plasma compression cycle is modeled by a sinusoidal modulation of the plasma length,

$$l = l_0[1 + \epsilon \sin(2\pi f t)], \tag{10}$$

where $l_0\epsilon$ is the amplitude of the modulation. Equations (8), (9) and (10) are solved by performing a perturbation expansion in small ϵ. To order ϵ^2, we find that

$$\left\langle \frac{dT}{dt} \right\rangle_{\text{cycle}} = \left(\frac{4\epsilon^2 \nu}{3} \frac{\beta^2}{1+\beta^2} - \frac{1}{\tau_r} \right) T, \tag{11}$$

where $T = (T_\parallel + 2T_\perp)/3$, the scaled frequency $\beta = 2\pi f/(3\nu)$, and $\langle dT/dt \rangle_{\text{cycle}}$ denotes an average of dT/dt over one modulation cycle. We assume $(f\tau_r)^{-1} \ll 1$. Thus, the average temperature T slowly changes in response to the competition between compressional heating and cyclotron radiation cooling. For a single cycle, the temperature change is

$$\Delta T = \left(\frac{8\pi\epsilon^2}{9} \frac{\beta}{1+\beta^2} - \frac{1}{f\tau_r} \right) T. \tag{12}$$

The maximum heating per cycle occurs when $\beta = 1$ (i.e. $2\pi f = 3\nu$).

Experimentally, we measure the heating per cycle by cyclically compressing the plasma for a fixed number of cycles H. After the compression cycles are over, we measure the parallel temperature of the plasma, T_e. In order to consistently obtain the same amount of cyclotron cooling independent of f, the temperature is always measured at a fixed time after the start of the heating cycles. We have tested Eq. (12) by constructing a plot of the final temperature T_e versus the compression frequency f, as shown in Fig. 5. Each point in this figure is obtained with a new, but initially identical, plasma. The line is calculated by iterating Eq. (12) H times. As Eq. (12) is iterated, the plasma temperature changes, thereby changing both the collision frequency ν and the scaled frequency β. Consequently we recalculate ν after each iteration using the modified Ichimaru–Rosenbluth formula $\nu(T) = \mathcal{C} n b^2 \bar{v} \log(r_c/b)$ [see Section IV B]. Using $\mathcal{C}$ and ϵ as free parameters, the iterated Eq. (12) is then least-square fit to the data, yielding $\epsilon = 0.053$ and $\nu = 36.3 \times 10^3$ Hz for $T = 1400$ K. We have also tested Eq. (12) with a slightly different experimental method; instead of heating for a fixed number of cycles, we heat for a fixed time t_h. The number of heating cycles, $f \times t_h$, now depends on f. The results of this test are given in Fig. 6. The theoretical prediction given by the solid line is determined as in the previous figure. For the data in Figs. 5 and 6, $\langle n \rangle \approx 7 \times 10^8$ cm^{-3} and $B = 61.3$ kG. The data in Fig. 5 were taken with $H = 80$ cycles and the data in Fig. 6 were taken with

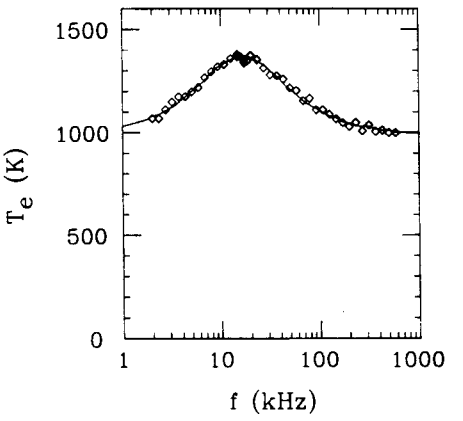

FIG. 5. Plasma temperature after heating T_e vs. compression frequency f. Heating comprised of $H = 80$ contiguous cycles. The points are experimental data and the solid curve is a prediction of the model.

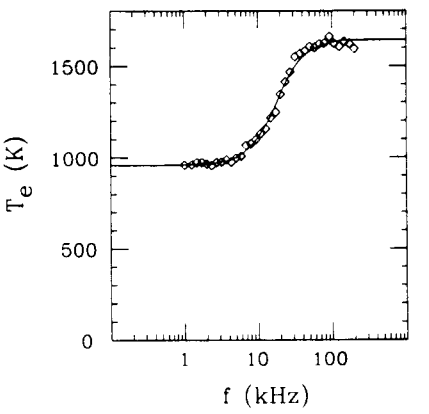

FIG. 6. Plasma temperature after heating T_e vs. compression frequency f. Heating for a fixed time, $t_h = 4$ ms. The points are experimental data and the solid curve is a prediction of the model.

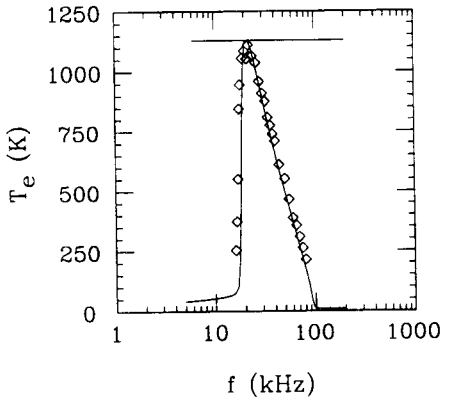

FIG. 7. Plasma temperature after heating T_e vs. compression frequency f using balanced heating technique.

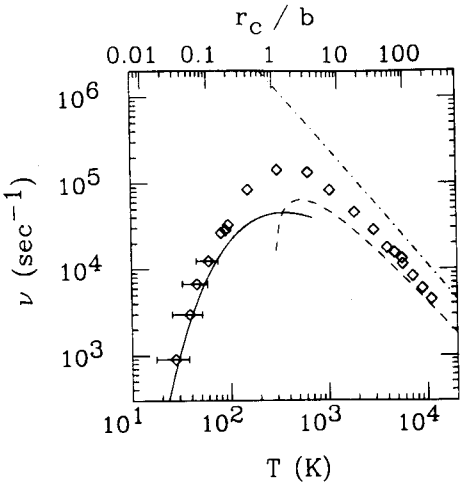

FIG. 8. Measured relaxation rate ν vs. temperature T and r_c/b for a magnetic field of 61.3 kG. The solid curve is the O'Neil–Hjorth prediction. The dashed curve is the modified Ichimaru–Rosenbluth prediction and the dot-dashed curve is the unmodified Ichimaru–Rosenbluth prediction.

$t_h = 4$ ms. In both figures T_e was measured 50 ms after the start of the heating process.

Other irreversible heating processes exist which are not included in our model. For example, plasma waves launched by the compression cycles could, through various damping processes, transfer their wave energy into plasma kinetic energy. However, we feel that Figs. 5 and 6 demonstrate that, at least for certain parameter ranges, other irreversible process can be ignored and that Eqs. (8) and (9) adequately describe our experiment.

The dependence of ν on T can be determined by repeating the method outlined in the description of Fig. 5 for a series of base temperatures. This technique works best at high plasma temperatures, and was used to obtain the square points plotted in Fig. 1. Unfortunately, the technique is not well suited to the low temperature regime because the temperature diagnostic becomes increasingly noisy. In addition, the relatively large temperature excursions required to obtain a reasonable peak (almost 40% in Fig. 5), coupled with the increasingly strong dependence of ν on T found at low temperatures, makes the assumed functional form of $\nu(T)$ overly critical. Consequently, we developed a more complex scheme ("balanced heating") that makes the heating peak sharper, while effectively reducing the temperature excursion. This scheme consists of subjecting each plasma to S heating intervals, each interval having H compression cycles and lasting for a fixed time that is short compared to the cyclotron radiation time. The total time and the total number of cycles remain independent of f. Furthermore, we take curves of T_e versus f for various compression amplitudes ϵ until an ϵ is found such that, at the heating peak, the plasma maintains a nearly constant temperature throughout the heating process. That is, for the appropriate ϵ, heating exactly balances cyclotron cooling when $2\pi f \simeq 3\nu$. When $2\pi f \neq 3\nu$, cyclotron cooling will always be stronger than compressional heating, and the plasma cools. Since the heating process lasts many cyclotron cooling times, the temperature drops sharply even for a slightly mismatched heating frequency. Data taken with this process are shown in Fig. 7, in which $S = 301$, $H = 24$ and each interval lasted 5 ms. The initial temperature of 1130 K is indicated by the horizontal line. The theoretically predicted response is obtained by numerically integrating Eqs. (8), (9) and (10) with Glinsky *et al.*'s formula[7] for $\nu(T)$ with the only fitted parameter being ϵ. This prediction is given only to show how well Eqs. (8), (9) and (10) model the experiment, and is not used to determine ν. The collision frequency ν is measured by determining the frequency f_{max} which maximizes the temperature T_e and then employing the formula $\nu = 2\pi f_{max}/3$. In their appropriate regimes, both the original and the balanced heating process yield values of ν that are precise to about 5%.

A. Results

In Fig. 8 we plot the measured collision frequency ν versus T (and r_c/b) for $B = 61.3$ kG along with several theoretical predictions. In Fig. 9 we plot ν versus T for magnetic fields of 30.7, 40.9 and 61.3 kG. The data in Figs. 8 and 9 were taken using the balanced heating process. The plasma parameters for this data are density $\langle n \rangle \simeq 8 \times 10^8$ cm^{-3}, length $l \simeq 3.5$ cm and $(T_\parallel - T_\perp)/T_\parallel \lesssim 4\%$ throughout

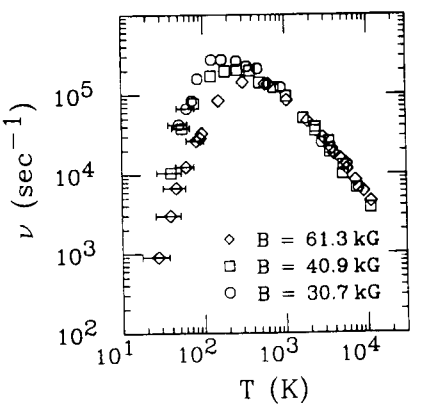

FIG. 9. Measured relaxation rate ν vs. temperature T for various magnetic fields. The plasma density for this data was approximately 8×10^8 cm^{-3}.

the heating process. In Fig. 1 this data is gathered with high temperature measurements using the original heating process, the results of Hyatt, Driscoll and Malmberg,[5,6] and the Monte Carlo prediction of Glinsky *et al.*[7] To within experimental error, the experimental data in Fig. 1 are described by Glinsky's prediction.

B. Theory

Many theoreticians have worked on the general problem of collisional processes in plasmas. While there are many interrelated collisional processes (resistivity, diffusion, Maxwellianization, etc.), we are principally concerned with the specific collisional process of temperature isotropization. In the standard high temperature regime $r_c > b$, Ichimaru and Rosenbluth[18] employ a Fokker–Planck formalism to calculate the relaxation rate for singly-ionized ions in a weakly magnetized, neutral plasma. Their prediction is trivially adapted to pure-electron plasmas. Furthermore, theoretical work by Silin[19] and theoretical/numerical work by Montgomery *et al.*[20] have shown that this low magnetic field theory (i.e. $r_c \gg \lambda_D \gg b$) can be applied to the high magnetic field regime $\lambda_D \gg r_c \gg b$ by changing the argument of the coulomb logarithm factor, Λ, from $\Lambda = \lambda_D/b$ to $\Lambda = r_c/b$. Here λ_D is the Debye length. Thus the suitably modified Ichimaru-Rosenbluth prediction for the collision frequency is

$$\nu = \frac{8\sqrt{\pi}}{15} n b^2 \bar{v} \log(\Lambda). \tag{13}$$

Since this formula is derived using the dominant-term approximation, it is valid only when $\log(\Lambda) \gg 1$.

In the low temperature, high magnetic field regime $\lambda_D \gg b \gg r_c$, O'Neil[21] argues that a many electron adiabatic invariant exists which suppresses scattering between parallel and perpendicular energy. When $b \gg r_c$, the collision time is so much slower than the gyroperiod (Ω^{-1}) that the time scale separation inhibits the transfer of energy. O'Neil finds that the total perpendicular action $[\Sigma(m v_\perp^2/2)/B$, where the sum is over all electrons] is an adiabatic invariant. In this regime O'Neil and Hjorth[4] calculate ν to be

$$\nu \simeq 2.48 n b^2 \bar{v} (r_c/b)^{1/5} \exp[-2.34 (b/r_c)^{2/5}]. \tag{14}$$

Glinsky *et al.*[7] refined these calculations to include the intermediate temperature regime $r_c/b \sim 1$. They postulate that only collisions with impact distances of order r_c and less contribute significantly to ν when $r_c \lesssim \lambda_D$. When $r_c < n^{-1/3}$ and the plasma is weakly correlated, a Boltzmann-like collision operator can be employed to calculate ν. For $(T_\parallel - T_\perp)/T_\parallel \ll 1$, they conclude that

$$\nu = \frac{n}{16} \int_0^\infty 2\pi p dp \int |u_\parallel| f_r(u_\parallel, u_\perp) \left(\frac{\Delta W_\perp}{T} \right)^2 d^3u, \tag{15}$$

where p is the impact distance, u is the relative velocity between two electrons, f_r is the relative velocity distribution, and $\Delta W_\perp$ is the change in the perpendicular energy. Because the magnetic field affects the orbits of the electrons, an analytic expression for $\Delta W_\perp$ cannot be obtained. Instead, $\Delta W_\perp$ is found numerically for many initial conditions chosen at random, and the integrals in Eq. (15) are numerically evaluated using Monte Carlo techniques.

C. Uncertainties in measured relaxation rate

Both the theoretical calculations of the relaxation rate and our model of the relaxation rate measurement technique assume that the perpendicular and parallel velocities are Maxwellianized. Since we measure ν by cyclically compressing the plasma, we risk modifying these velocity distributions. This risk is greatest in the regime $r_c/b \ll 1$ where theory predicts that the dominant contribution to ν comes from the small number of electrons in the tail of the Maxwellian (i.e. $v_\parallel \approx \bar{v}(3\pi b/r_c)^{1/5}$). However, we believe that the compression cycles do not significantly alter the distribution for the following reasons: first, simple one-dimensional (1-d) longitudinal compressions of the plasma preserve Maxwellian distributions. Second, the compression amplitude is small. Third, since $\nu \sim f$, re-Maxwellianization occurs on the same time scale as compressions might attempt to alter the distribution. Fourth, in the balanced heating process the heating is broken up into heating and nonheating phases. Since the heating duty cycle is only about 50%, and since each nonheating phase lasts about 50 relaxation times ν^{-1}, there should be ample time for the plasma to re-Maxwellianize during the nonheating phase.

At each temperature, we can determine the frequency which produces the most heating per cycle to within about 5%. If the average heating per electron at radius r were independent of r and if the density were uniform, then ν would also be determined to about 5%. However, since $\nu \propto n$ and the heating depends on the ratio ν/f, radial density variations cause a radial variation in the heating per electron and add additional uncertainty to our results. To estimate this uncertainty, we have analyzed our heating procedure for various density profiles. Since we do not know the radial thermal conductivity of our plasmas, we studied both zero and infinite radial thermal conductivity. The error bars in our figures include the uncertainty predicted by this analysis.

To derive Eq. (11) we assumed that ϵ is small. For the simple heating process the fitting routine yields a good estimate of ϵ. For the balanced heating process, ϵ is easily estimated by using the fact that at the optimal heating frequency, the average heating ($\sim 4\pi H \epsilon^2 T/9$) balances the average cooling ($\sim t_i T/\tau_r$) for each interval. Here t_i is the time per interval. We conclude that $\epsilon \lesssim 0.06$ and that corrections to ν due to finite ϵ are at most 5%.

Accurately determining $\nu(T)$ requires us to accurately measure the temperature T. Because of the strong dependence of ν on T in the regime $r_c/b < 1$, the possible systematic error of 30% in the measured temperatures in this region is much more important than the uncertainties in the measured ν when comparing theory to experiment.

V. SUMMARY

We have measured pure-electron plasma temperatures between 25 and 2×10^6 K. We have also measured the anisotropic thermal relaxation rate ν for $1/35 \lesssim r_c/b \lesssim 2 \times 10^5$.

For $r_c/b \gg 1$ our results are consistent with the theory of Ichimaru and Rosenbluth, modified for a strong magnetic field. For $r_c/b \ll 1$, our results are consistent with O'Neil and Hjorth's prediction that the collisional dynamics is modified by a many electron adiabatic invariant. Finally, for $r_c/b \sim 1$, our results agree with the prediction by Glinsky *et al.*

ACKNOWLEDGMENTS

The authors thank Dr. C. F. Driscoll, Dr. M. E. Glinsky, Dr. P. H. Hjorth, Dr. A. J. Peurrung, and Professor T. M. O'Neil.

This work was supported by the National Science Foundation under Grant No. PHY87-06358, and by the Office of Naval Research.

APPENDIX A: DENSITY MEASUREMENT

We infer the plasma density from its line integrated charge. This charge is determined by measuring the number of electrons which flow onto the charge collectors **C** when the plasma is released by grounding the end electrode $\mathbf{G}_3$. Each collector $\mathbf{C}_i$ all the plasma electrons between radius r_i and r_{i+1},

$$N_i = 2\pi \int_{r_i}^{r_{i+1}} \aleph(r) r dr, \tag{A1}$$

where r_j is the radius of the hole in $\mathbf{C}_j$ (note that $r_1 = 0$ cm and $r_6 = R_w$) and $\aleph(r) = \int n(r,z) dz$ is the line integrated density at radius r. Typically, about 99% of the electrons are collected onto $\mathbf{C}_1$ and $\mathbf{C}_2$ (with $N_1 \simeq N_2$); thus, little can be inferred about the radial dependencies of $\aleph(r)$ or $n(r,z)$. However, using Poisson's equation, the known boundary conditions and an assumed radial line density profile,[23,24] we can estimate the average density $\langle n \rangle$, and average axial length l, to about 15%.

We can obtain better radial resolution by lowering the magnetic field prior to releasing the plasma. Since the plasma column rotation frequency is much greater than the rate at which we lower the field, the flux enclosed by the plasma, Br^2, is an adiabatic invariant and the plasma expands radially in a predictable manner. Consequently the line integrated density measured after the expansion, $\aleph_a(r)$, is related to line density before the expansion, $\aleph_b(r)$, by $\aleph_a(r) = \alpha^2 \aleph_b(\alpha r)$ where $\alpha = \sqrt{B_a/B_b}$ and B_b (B_a) is the field before (after) the field ramping. Thus a significant fraction of the expanded plasma can be made to fall onto the outer charge collectors. For one typical setup we obtain an $\aleph(r)$ which is well approximated by $\aleph(r) = \aleph(0) \times \exp[-(r/0.048 \text{ cm})^3]$. In our analysis of the uncertainties in the measured relaxation rate and in the measured temperature, we use line densities of the form $\aleph(r) = N \exp[-(r/a)^p]$ where $1 < p < 5$.

APPENDIX B: TEMPERATURE MEASUREMENT

Normally, the electrons in our plasmas are so well confined that even the most energetic electrons do not have sufficient energy to escape over the potential barriers at the plasma ends. By measuring the number of electrons that escape as one of these potential barriers is slowly decreased, we can determine the plasma temperature.[25]

In practice, we lower the potential barrier created by $\mathbf{G}_3$ by slowly reducing the bias V_3. Only electrons with sufficient parallel kinetic energy escape; thus $v_\parallel$ must be greater than the escape velocity $v_e(r,V_3)$, defined by the relation

$$\frac{m v_e^2(r,V_3)}{2} \equiv -e[V_3 - \Phi(r,V_3)]. \tag{B1}$$

Here $\Phi(r,V_3)$ is the potential at radius r created by both the plasma space charge and the electrodes. For simplicity, we evaluate $\Phi(r,V_3)$ at the plasma axial midplane where the confining potentials are negligible, thus, to a good approximation, $\Phi(r,V_3)$ is just the electron space charge potential. However, $\Phi(r,V_3)$ is still a function of V_3 since the space charge changes as electrons escape.

If V_3 is decreased sufficiently slowly,[26] essentially all electrons at r with axial velocity $v_\parallel(r) > v_e(r,V_3)$ escape while all other electrons remain confined. Assuming that the electrons are in thermal equilibrium, the number of electrons at a given radius r which escape is proportional to the integral of the Maxwellian distribution from $v_\parallel = v_e(r,V_3)$ to $v_\parallel = \infty$, and equals $\text{erfc}[v_e(r,V_3)/\sqrt{2}\,\bar{v}]$, where erfc is the complementary error function. The total number of electrons $N_1(V_3)$ collected on $\mathbf{C}_1$ is found by integrating this error function weighted by the line density over the area bounded by $r = r_1$,

$$N_1(V_3) = 2\pi \int_0^{r_1} \aleph(r) \text{erfc}[v_e(r,V_3)/\sqrt{2}\,\bar{v}] r\, dr. \tag{B2}$$

The escaped charge $N_1(V_3)$ is most sensitive to the plasma temperature if only electrons in the tail of the electron distribution are allowed to escape. When $y = v_e(r,V_3)/\bar{v} \gg 1$ we can asymptotically expand the complementary error function to show that

$$\frac{1}{e} \frac{d \log N_1(V_3)}{dV_3} = \frac{1}{\kappa T} \left(1 + \frac{1}{2} \left\langle \frac{1}{y^2} \right\rangle \right) \tag{B3}$$

to order $\langle 1/y^4 \rangle$, where $\langle 1/y^p \rangle$ is defined as

$$\langle 1/y^p \rangle \equiv \frac{\int_0^{r_1} (1/y^p) \aleph(r) \text{erfc}(y) r dr}{\int_0^{r_1} \aleph(r) \text{erfc}(y) r dr}. \tag{B4}$$

Here we have ignored changes to $\Phi(r,V_3)$ due to the escaping electrons (i.e. we have set $d\Phi(r,V_3)/dV_3 = 0$). When $v_e(0,V_3)/\bar{v} \gtrsim 2$ we can show that $\langle 1/y^2 \rangle / 2 \lesssim 0.10$, independent of the functional form of $\aleph(r)$ for reasonable $\aleph(r)$. Thus, so long as only tail electrons are analyzed [i.e. $(v_e(0,V_3)/\bar{v} \gtrsim 2)$], Eq. (B3) simplifies to

$$\frac{1}{e} \frac{d \log N_1(V_3)}{dV_3} = \frac{1.05}{\kappa T}, \tag{B5}$$

which is accurate to about $\pm 5\%$, and can be used to determine the temperature T. Figure 10 shows a plot of N_1 and $\log_{10}(N_1)$ versus V_3 for a high temperature plasma. In general, the straight line region of $\log_{10}(N_1)$ where Eq. (B5) is valid extends for about one decade in N_1 at a temperature of

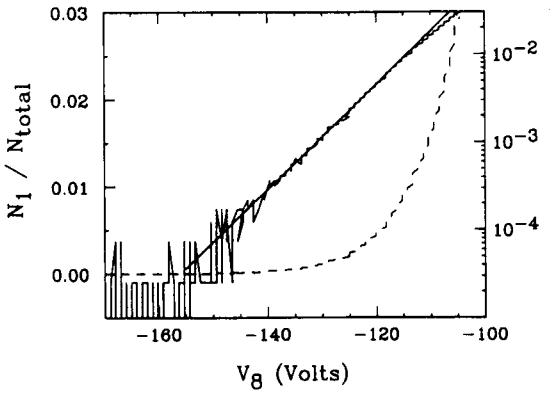

FIG. 10. Normalized number of escaped electrons N_1/N_{total} (dash curve) and $\log_{10}(N_1/N_{\text{total}})$ (solid curve) vs. V_3 taken for the high temperature analysis. Here N_{total} is the total number of confined electrons. The temperature determined from the straight line region of $\log_{10}(N_1)$ is 9.0×10^4 K. The solid, straight line through the $\log_{10}(N_1)$ curve is drawn to aid the eye. Digitization effects can be seen in both curves.

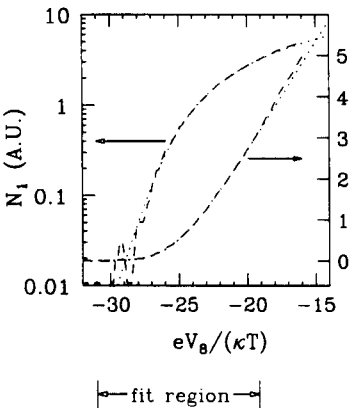

FIG. 11. Normalized number of escaped electrons N_1 vs. $eV_3/(\kappa T)$ taken for the low temperature analysis, displayed on logarithmic (left) and linear (right) axis. The dash curves are the measured N_1 and the dot curves are the fitted $C_0 l N_{\text{model}}$.

1000 K and about three decades in N_1 at higher temperatures. Noise and the tail electron condition $[v_e(0,V_3)/\bar{v}) \gtrsim 2]$ limits the region.

Below 500 K, the above method fails because the required straight-line region is no longer observable, as can be understood by the following argument. In general, as the confinement barrier is lowered, electrons escape from the radial center of the plasma first because the plasma space charge causes the effective confinement barrier potential there to be the lowest. Since the potential across the plasma increases with radius as $\pi n e r^2$, the effective confinement barrier potential will increase in height by one κT of energy in a distance $(\kappa T/\pi n e^2)^{1/2} = 2\lambda_D$. Consequently, only the tail electrons within a few Debye lengths of the radial center escape before the signal is contaminated by escaping bulk (i.e. non-tail) electrons. Since the Debye length decreases with plasma temperature, the number of tail electrons available for analysis likewise decreases.[27] Below about 500 K, the signal produced by these tail electrons is not sufficiently greater than our amplifier noise, and the straight line analysis of Eq. (B5) fails.

Bulk electrons still contain some temperature information. If we relax the condition that $v_e(0,V_3)/\bar{v} \gtrsim 2$ to $v_e(0,V_3)/\bar{v} \gtrsim 0.5$, we can employ about 50 times as many electrons in our analysis, with a correspondingly improved signal to noise ratio. However, the approximations used to derive Eq. (B5) are no longer valid. It remains true that most of the escaping electrons satisfying the new condition come from the plasma's central core; virtually all from within a radius $r = 10\lambda_D$. At low temperatures the region bounded by $r = 10\lambda_D$ is a small fraction of the total plasma; consequently we assume that both $n(r)$ and $\aleph(r)$ are uniform over this region. We then fit our data to the formula for the escaped charge given by Eq. (B2). The computerized fitting routine[12] minimizes the least squares sum

$$\sum [N_{\text{data}}(V_3) - C_0 l N_{\text{model}}(V_3') + C_1]^2, \tag{B6}$$

where N_{model} is the number of escaped electrons per unit length, $V_3' = (V_3 - \Phi_c)/(\kappa T)$, by varying the parameters C_0, C_1, T and Φ_c. The sum is over a window in the data chosen by the experimentalist. The parameter C_1 removes any offset in the data, and the parameter Φ_c is the potential at $r = 0$ due to the plasma charge. Figure 11 shows a plot of N_{data} (dashed curve) and $l C_0 N_{\text{model}}$ (dotted curve) versus V_3 for a low temperature plasma. For 500 K $\lesssim T \lesssim$ 2000 K we find that this fitting procedure and the simplified formula Eq. (21) yield the same T to within 5%. However, we use the simplified formula whenever possible since it is easier to apply and significantly faster to compute.

In the above discussion we assume that the temperature does not depend on the radius. If we rederive Eq. (B3) while allowing T to be a function of radius, we find that the measured temperature is a weighted radial average of $T(r)$. Since virtually all of the electrons which we analyze come from the region inside $r = 10\lambda_D$, and since we only monitor the charge collected on $\mathbf{C}_1$, we effectively measure the average temperature of the electrons between $r = 0$ and the minimum of $10\lambda_D$ and r_1. When the temperature is low, the region bounded by $r = 10\lambda_D$ is a small fraction of the total plasma; thus, for low temperatures the measured temperature is essentially the on-axis temperature.

For high temperatures, estimates of the maximum radial temperature variation can be obtained by observing the signals on $\mathbf{C}_1$ and $\mathbf{C}_2$ simultaneously as the voltage on V_3 is slowly ramped to ground. The equation for the number of electrons collected on $\mathbf{C}_2$ as a function of V_3 is similar to Eq. (B2). Hence, for sufficiently high temperatures, $(1/e) d \log N_2/dV_3 \approx 1.05/(\kappa T)$, provided restriction similar to those used in deriving Eq. (B5) hold. We find that temperatures derived from the N_1 and N_2 signals agree to within 10%.

For temperatures above 200 K we believe the error in the temperature measurement to be about 10%. This error increases as the temperature decreases below $T \approx 200$ K. At $T \approx 30$ K the random error is about 30%, and there may be a systematic error of about 30%. An independent test of the parallel temperature $T_\parallel$ measurement was done by

Hyatt[6] using a similar pure-electron apparatus. The perpendicular temperature $T_\perp$ can be measured on his apparatus to about 5% accuracy. For plasmas in thermal equilibrium, Hyatt found that their measured $T_\parallel$ and $T_\perp$ agreed to within 10%.

In this discussion, we have ignored the fact that the actual confinement potential barrier is less than the applied voltage V_3 because electrode $\mathbf{G}_3$ is finite in length. We have also ignored the fact that the plasma expands and cools during the measurement. Corrections for both of these phenomena are included in the actual analysis of the data.

APPENDIX C: HYATT, DRISCOLL AND MALMBERG RESULTS

Hyatt *et al.*[5,6] used a pure-electron plasma trap similar to ours. However, their magnetic field was much lower ($\sim$280 G), their plasma temperatures were generally higher ($\sim 10^4$ K) and their plasma densities were lower ($\sim 10^7$ cm^{-3}). Consequently, their plasmas are in the regime $3\times 10^4 \lesssim r_c/b \lesssim 10^6$, with $\lambda_D/r_c \approx 30$. They measure ν by first forming a plasma with equal $T_\parallel$ and $T_\perp$. They then change $T_\parallel$ by quickly compressing or expanding the plasma axially, leaving $T_\perp$ unchanged. They determine the relaxation rate from the subsequent time evolution of $T_\parallel$ and $T_\perp$ as these temperatures relax to a new common value. They measure the relaxation rate as a function of density and temperature over a two decade range, with an uncertainty of about 10%. They compared their data to the Ichimaru–Rosenbluth prediction and found agreement to about 10%.

[1] *Non-Neutral Plasma Physics*, edited by C. W. Roberson and C. F. Driscoll, AIP Conf. Proc. 175 (American Institute of Physics, New York, 1988).
[2] *Non-Neutral Plasma Physics II*, edited by J. Fajans and D. H. E. Dubin, AIP Conf. Proc. 331 (American Institute of Physics, New York, 1995).
[3] R. S. Cohen, L. Spitzer, and P. McRoutly, Phys. Rev. **80**, 230 (1953), and references therein.
[4] T. M. O'Neil and P. G. Hjorth, Phys. Fluids **28**, 3241 (1985).
[5] A. W. Hyatt, C. F. Driscoll, and J. H. Malmberg, Phys. Rev. Lett. **59**, 2975 (1987).
[6] A. W. Hyatt, Ph.D. thesis, University of California, San Diego, 1988.
[7] M. E. Glinsky, T. M. O'Neil, M. N. Rosenbluth, K. Tsuruta, and S. Ichimaru, Phys. Fluids B **4**, 1156 (1992).
[8] T. M. O'Neil, Phys. Fluids **23**, 2216 (1980).
[9] The filament is actually placed beyond the end of the solenoidal magnet, where the field strength is about 1/20 of the central field value. Electrons are forced into the higher magnetic field region by biasing the filament sufficiently negative.
[10] C. F. Driscoll, K. S. Fine, and J. H. Malmberg, Phys. Fluids **29**, 2015 (1986).
[11] X. P. Huang, K. S. Fine, and C. F. Driscoll, Phys. Rev. Lett. **74**, 4424 (1995).
[12] B. R. Beck, Ph.D. thesis, University of California, San Diego, 1990.
[13] The confinement electrodes form a cylindrical waveguide which would cut off cyclotron radiation for magnetic fields less than 3.2 kG.
[14] G. Gabrielse and J. Tan, in *Advances in Atomic, Molecular and Optical Physics, Supplement 2*, edited by P. R. Berman (Academic, Boston, 1994), p. 267.
[15] D. H. E. Dubin and T. M. O'Neil, Phys. Rev. Lett. **56**, 167 (1986).
[16] Note that during the compression the potential pressure indirectly affects the kinetic pressure through the self-consistent balance of forces that determine the plasma length.
[17] D. L. Book, *NRL Plasma Formulary* (Office of Naval Research, Washington, DC, 1987).
[18] S. Ichimaru and M. N. Rosenbluth, Phys. Fluids **13**, 2778 (1970).
[19] V. P. Silin, Sov. Phys. JETP **14**, 617 (1962).
[20] D. Montgomery, G. Joyce, and L. Turner, Phys. Fluids **17**, 2201 (1974).
[21] T. M. O'Neil, Phys. Fluids **26**, 2128 (1983).
[22] S. A. Prasad and T. M. O'Neil, Phys. Fluids **22**, 278 (1979).
[23] A. J. Peurrung and J. Fajans, Phys. Fluids B **2**, 693 (1990).
[24] D. L. Eggleston, C. F. Driscoll, B. R. Beck, A. W. Hyatt, and T. H. Malmberg, Phys. Fluids B **4**, 3432 (1992).
[25] For an electron with $v_\parallel = \bar{v}$ the word slow means $d(eV_3)/dt \ll T(\bar{v}/l)$. This definition of slow insures that when an electron escapes, its axial energy at the hill's peak is much smaller then κT; thus all electrons at the same radial position and axial energy escape at essentially the same V_3. However, the barrier must be changed quickly compared to the collision time and any radial transport times.
[26] The number of electrons that escape within a few λ_D is proportional to $n\lambda_D^2 l \propto Tl$, and is independent of the density n.